Available online at www.sciencedirect.com
SCIENCE DIRECT®
Remote Sensing of Environment 86 (2003) 423–432
Remote Sensing of Environment
www.elsevier.com/locate/rse

Solar energy assessment using remote sensing technologies

Annette Hammer[a], Detlev Heinemann[a], Carsten Hoyer[a,*], Rolf Kuhlemann[a], Elke Lorenz[a], Richard Müller[a], Hans Georg Beyer[b]

[a] *Department of Energy and Semiconductor Research, Faculty of Physics, University of Oldenburg, D-26111 Oldenburg, Germany*
[b] *Department of Electrical Engineering, University of Applied Sciences (FH) Magdeburg-Stendal, D-39114 Magdeburg, Germany*

Received 13 March 2002; received in revised form 26 September 2002; accepted 28 December 2002

Abstract

About 20% of the final energy consumed in Europe is used in buildings. The active and passive use of solar energy is an approach to reduce the fossil energy consumption and the greenhouse gas emissions originated by buildings. Consideration of solar energy technologies in urban planning demands accurate information of the available solar resources. This can be achieved by the use of remote sensing data from geostationary satellites which show a very high spatial and a sufficient temporal resolution compared to ground station data. This paper gives a brief introduction to the HELIOSAT method applied to derive surface solar irradiance from satellite images and shows examples of applications: The use of daylight in buildings, the generation of correlated time series of solar irradiance and temperature as input data for simulations of solar energy systems and a short-term forecast of solar irradiance which can be used in intelligent building control techniques. Finally an outlook is given on potential improvements expected from the next generation of European meteorological satellites Meteosat Second Generation (MSG).

Keywords: Solar energy; Remote sensing; HELIOSAT

1. Introduction

About 20% of the final energy consumed in Europe is used in buildings. The European Commission expects in its Green Paper on the security of energy supply (Commission of the European Communities, 2000) that a "greater use of available and economically viable energy-efficient technologies should reduce the use of energy in buildings by at least a fifth, that is 40 million toe[1] per year." This reduction would be equivalent to 4% of the total energy use and thus about a fifth of the CO_2 reduction committed in the Kyoto protocol. An additional use of renewable energy sources would further reduce the emissions.

Solar energy can be used in buildings and urban environments in various—active and passive—ways. Active applications use solar thermal collectors for heating and cooling or use photovoltaic (PV) generators, built upon rooftops or integrated into building facades, for electricity production. Passive uses of solar energy mean designing buildings and their windows in a way that they use solar radiation for heating and illumination. Not only buildings but whole settlements may benefit from a solar design: Large collector arrays can be used to produce local heat and large PV arrays can produce a significant share of the settlement's electricity demand.

An accurate knowledge of the solar resource at the surface is essential for a successful introduction of solar energy technologies in the urban environment. The data can be used to simulate the performance of solar energy systems and is needed to optimize the layout and size of the systems. It also can be used to simulate the thermal performance of buildings aiming at an optimum design for heating and cooling. Knowledge of the local conditions is also important for the use of daylight in buildings. Correct design of the buildings can lower the use of artificial light and thus reduce energy demand and make the working conditions within the room more comfortable.

Efficient use of the solar resource not only requires appropriate design of buildings and solar components, but

* Corresponding author. New affiliation German Aerospace Center, Institute of Technical Thermodynamics, Pfaffenwaldring 38-40, Stuttgart D-70569, Germany. Tel.: +49-711-6862-784; fax: +49-711-6862-783.
E-mail address: carsten.hoyer@dlr.de (C. Hoyer).
[1] One ton of oil equivalent (toe) equals approximately 42 GJ.

0034-4257/03/$ - see front matter © 2003 Elsevier Science Inc. All rights reserved.
doi:10.1016/S0034-4257(03)00083-X

also sophisticated system management. Energy efficient buildings will use intelligent control techniques to coordinate needs of consumers and resources with respect to energy consumption, lighting and climate control of buildings. This implies information on the temporal development of the system and the meteorological conditions influencing the system. Forecasting solar radiation thus will become an important issue for an optimized use of solar energy in the future.

Ground measured solar radiation is scarcely available for a given site where a solar system is planned—the measurement network's density is usually far too low. Geostationary satellites such as METEOSAT provide the opportunity to derive information on solar irradiance for a large area at a temporal resolution of up to 30 min and a spatial resolution of up to 2.5 km. Derived hourly values have proven to be at least as good as the measurements of a ground station at a distance of 25 km (Zelenka, Perez, Seals, & Renne, 1999).

Several computational methods have been developed in the past two decades for estimating the downward solar irradiance from satellite observations (Renne, Perez, Zelenka, Whitlock, & DiPasquale, 1999). Here the HELIOSAT method is presented, which has been used in various European research projects to derive solar irradiance information for solar energy and daylight use. It has extensively been tested with ground data, e.g. in Beyer, Costanzo, and Heinemann (1996) and Hammer (2000). This paper presents examples from two of these projects. A further example shows the use of satellite-derived radiation data as a basis for short range forecasting.

Finally an outlook is given on potential improvements expected from the next generation of European meteorological satellites: Meteosat Second Generation (MSG).

2. The HELIOSAT method

The general idea of the HELIOSAT method for the estimation of surface solar irradiance from satellite images is to deal with atmospheric and cloud extinction separately. In a first step the clear sky irradiance for a given location and time is calculated. In a second step a cloud index is derived from METEOSAT imagery to take into account the cloud extinction. This step uses the fact that the reflected radiance measured by the satellite is approximately proportional to the amount of cloudiness characterized by the cloud index. This value then is correlated to the cloud transmission. Finally, the clear sky irradiance is reduced due to the cloud transmission to infer the surface irradiance. Fig. 1 gives an overview of the alogrithms to calculate the surface irradiance from a satellite image. The top and lefthand side corresponds to the first step and the righthand side to the second step.

Details of the algorithm as well as the derivation of additional quantities used in solar energy applications are described in the following sections.

2.1. Clear sky irradiance

The HELIOSAT method was originally proposed by Cano et al. (1986) and later modified by Beyer et al. (1996) and Hammer (2000). For the calculation of the clear sky irradiance a direct irradiance model of Page (1996) and a diffuse irradiance model of Dumortier (1995) are used. These models were developed by an empirical analysis of ground data. Both use the Linke turbidity factor to describe the atmospheric extinction. The direct normal irradiance G_{dn} is then given by:

$$G_{dn,clear} = G_{sc}\epsilon e^{-0.8662\cdot T_L(2)\delta_R(m)m} \tag{1}$$

where G_{sc} is the solar constant, ϵ is the eccentricity correction, $T_L(2)$ is the Linke turbidiy factor for air mass 2, $\delta_R(m)$ is the Rayleigh optical thickness and m is the air mass.

The eccentricity correction ϵ is given by:

$$\epsilon = 1.000110 + 0.034221\cos\Gamma + 0.001280\sin\Gamma + 0.000719\cos 2\Gamma + 0.000077\sin 2\Gamma \tag{2}$$

with

$$\Gamma = 2\pi\frac{J-1}{365}. \tag{3}$$

Here, J corresponds to the day of year.

Air mass is calculated using an expression introduced by Kasten and Young (1989):

$$m = \frac{1 - z/10000}{\cos\theta_z + 0.50572(96.07995 - \theta_z)^{-1.6364}}, \tag{4}$$

with the height z of the site in meters and the zenith angle θ_z of the sun in degrees. The Rayleigh optical thickness $\delta_R(m)$ is the optical thickness of a dry and clean atmosphere, where only Rayleigh scattering occurs. According to Kasten (1996) and Page (1996) for $m<20$ it can be approximated by:

$$\delta_R = \frac{1}{6.6296 + 1.7513\ m - 0.1202\ m^2 + 0.0065\ m^3 - 0.00013\ m^4} \tag{5}$$

and for $m>20$ by:

$$\delta_R = \frac{1}{10.4 + 0.718\ m}. \tag{6}$$

The Linke turbidity is defined as the number of Rayleigh atmospheres necessary to represent the actual optical thickness $\delta(m)$:

$$T_L = \frac{\delta(m)}{\delta_R(m)} \tag{7}$$

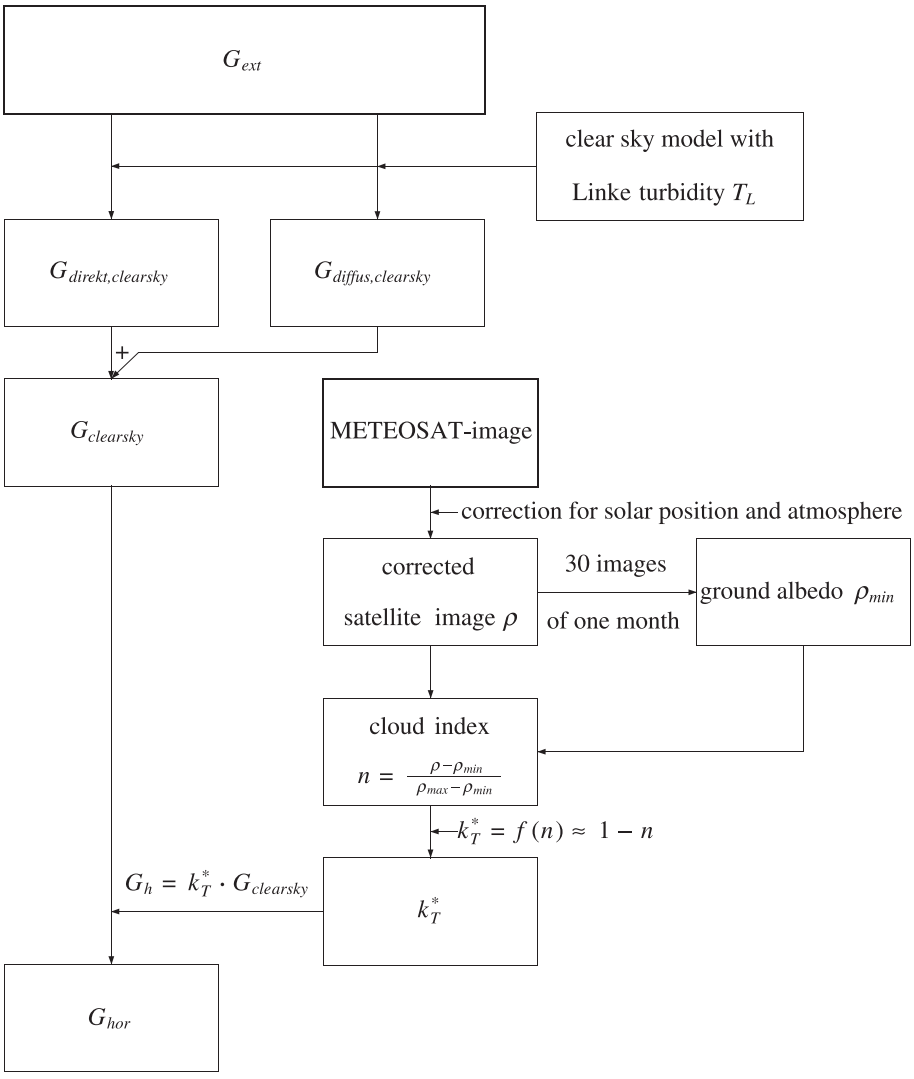

Fig. 1. Overview of the HELIOSAT method.

Since this turbidity still shows a daily variation, it is normalized to the turbidity for air mass 2:

$$T_{\mathrm{L}}(2) = \frac{T_{\mathrm{L}}(m)\delta_{\mathrm{R}}(m)}{\delta_{\mathrm{R}}(2)}. \tag{8}$$

The diffuse irradiance is calculated using an empirical relationship by Dumortier (1995):

$$G_{\mathrm{dif,clear}} = G_{\mathrm{ext}}\epsilon(0.0065 + (-0.045 + 0.0646T_{\mathrm{L}}(2))\cos\theta_{\mathrm{z}} + (0.014 - 0.0327T_{\mathrm{L}}(2))\cos^2\theta_{\mathrm{z}}). \tag{9}$$

G_{ext} is the extraterrestrial irradiance on a horizontal plane.

Since the spectral channels of METEOSAT do not supply any information on atmospheric turbidity, a climatological model is applied. To account for the annual variation of the turbidity a relation of Bourges (1992) is used:

$$T_{\mathrm{L}}(2) = T_0 + u\cos\left(\frac{2\pi}{365}J\right) + v\sin\left(\frac{2\pi}{365}J\right), \tag{10}$$

T_0, u and v are site specific parameters, A map specifying the parameters for Europe has been set up during the EU-funded *Satel-Light* project (http://www.satel-light.com).

Finally the total clear sky irradiance is the sum of the components:

$$G_{\mathrm{clear}} = G_{\mathrm{dn,clear}}\cos\theta_{\mathrm{z}} + G_{\mathrm{dif,clear}} \tag{11}$$

2.2. Cloud transmission

Clouds have the largest influence on atmospheric radiative transfer. The cloud amount is derived from METEOSAT imagery. First the METEOSAT images are normalized with respect to the solar zenith angle. Therefore a relative reflectance ρ is introduced:

$$\rho = \frac{C - C_0}{G_{\mathrm{ext}}}. \tag{12}$$

Here C is the measured pixel intensity of the satellite radiometer and C_0 is a total offset resulting from an instrument offset C_{off} and an atmospheric offset C_{atm} due to atmospheric backscattering. An empirical relationship for C_{atm} was derived from an analysis of ocean pixels:

$$C_{atm} = (1 + \cos^2 \Psi) \frac{f(\theta_z)}{\cos^{0.78} \phi}, \tag{13}$$

where Ψ is the angle between sun and satellite as seen from the ground and ϕ is the zenith angle of the satellite. Ocean pixels are used because the surface reflectance of oceans in the direction of the satellite can be neglected. The measured reflectance therefore nearly completely results from the atmosphere.

The function $f(\theta_z)$ is (Hammer, 2000):

$$f(\theta_z) = -0.55 - 25.2\cos\theta_z - 38.3\cos^2\theta_z + 17.7\cos^3\theta_z. \tag{14}$$

The total offset C_0 then is

$$C_0 = C_{off} + C_{atm}. \tag{15}$$

The measured reflectance is usually low for earth surfaces and high for clouds. Therefore a cloud index n as a measure of the cloud cover is introduced. It varies between 0 for cloud free and 1 for overcast conditions and uses the relative reflectivity ρ from Eq. (12):

$$n = \frac{\rho - \rho_{min}}{\rho_{max} - \rho_{min}}. \tag{16}$$

ρ_{min} corresponds to the surface albedo. Maps of the surface albedo are computed on a monthly basis by a statistical analysis of the dark pixels. The monthly calculation is done to account for seasonal variations of the ground reflectance. The maximum reflectivity ρ_{max} is computed separately for each satellite radiometer due to differences in the sensor properties in the different METEOSAT satellites (Hammer, Heinemann, & Hoyer, 2001).

Cloud transmission can be described by the clear sky index k_T^* which normalizes the actual surface irradiance G with the clear sky irradiance G_{clear} from Eq. (11):

$$k_T^* = \frac{G}{G_{clear}}. \tag{17}$$

The clear sky index k_T^* is calculated using a simple relationship with the cloud index n. The relationship is shown in Fig. 2. It has been derived within the *Satel-Light* project (Fontoynont et al., 1997, 1998):

$$\begin{aligned} n &\le -0.2 \quad & k_T^* &= 1.2 \\ -0.2 < n &\le 0.8 \quad & k_T^* &= 1 - n \\ 0.8 < n &\le 1.1 \quad & k_T^* &= 2.0667 - 3.6667n + 1.6667n^2 \\ 1.1 &< n \quad & k_T^* &= 0.05 \end{aligned} \tag{18}$$

Eqs. (11) and (17) are then used to obtain the surface irradiance G:

$$G = k_T^*(G_{dn,clear}\cos\theta_z + G_{dif,clear}) \tag{19}$$

The direct and diffuse irradiance are taken from Eqs. (1) and (9), respectively.

2.3. Direct and diffuse irradiance

For most solar energy applications the irradiance in the plane of the solar converter is of interest rather than global horizontal irradiance. For example, daylight applications often need data for vertically oriented planes. In these cases the fractions of direct and diffuse irradiance also have to be known to convert the horizontal irradiances to the tilted planes.

The direct and diffuse component of the surface irradiance is derived using a statistical model (Skartveit, Olseth, & Tuft, 1998) based on hourly values of the global irradiance. It

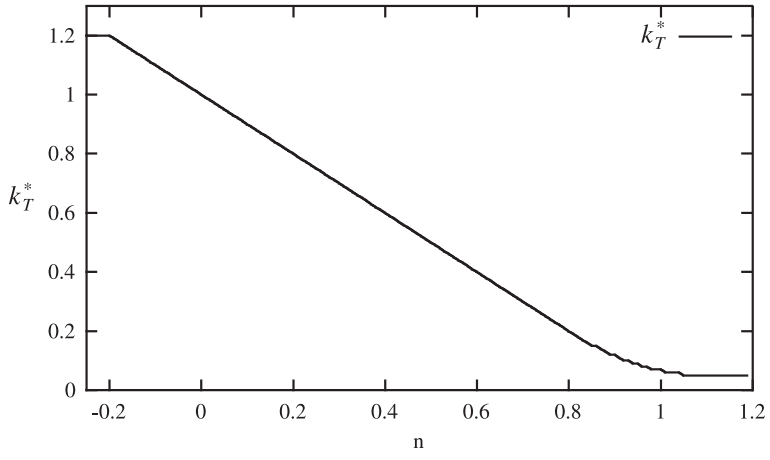

Fig. 2. Relation between cloud index n and clear sky index k_T^* used in the HELIOSAT method.

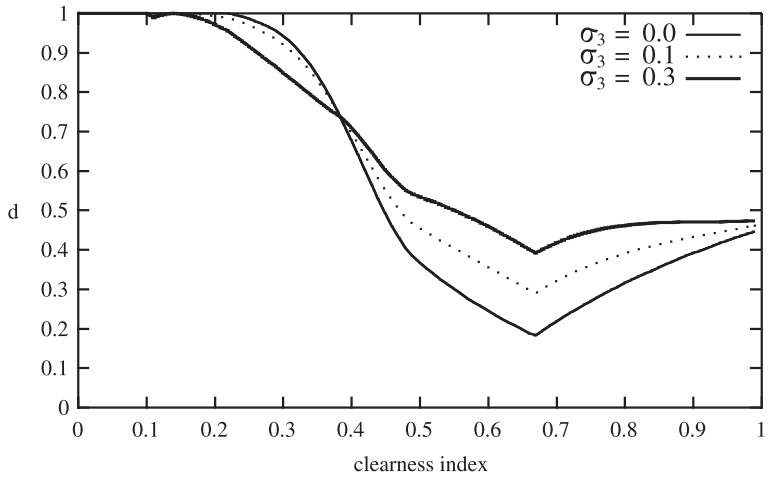

Fig. 3. Diffuse fraction d versus clearness index k_T and variability index $\sigma_3 = 0.0$, 0.1 and 0.3 for a solar zenith angle of 80° (Skartveit et al., 1998).

uses the clearness index k_T, the solar zenith angle and an hourly variability index σ_3 for the calculation of the diffuse fraction. The clearness index k_T is the global irradiance normalized with the extraterrestrial irradiance G_{ext}:

$$k_T = \frac{G}{G_{ext}}. \tag{20}$$

The hourly variability index σ_3 is determined from the clearness indices of three consecutive hours. If k_{T_i} is the clearness index of the hour i, then σ_3 is defined as:

$$\sigma_3 = \sqrt{\frac{(k_{T_i} - k_{T_{i-1}})^2 + (k_{T_i} - k_{T_{i+2}})^2}{2}}. \tag{21}$$

Figs. 3 and 4 show the diffuse fraction for two solar elevations. The expected decrease of the diffuse fraction with increasing clearness index reverses for large clearness index values. This is due to additional reflections by clouds especially under broken cloud conditions. The diffuse fraction is generally higher for large solar zenith angles, because of increased scattering due to the longer path length.

2.4. Illuminance

Illuminance is the radiant flux density from visible radiation. Illuminances are gained by weighting the global irradiance with the spectral sensitivity of the human eye. They form the most appropriate inputs for the analysis and optimization of architectural concepts to minimize the need of artificial lighting in buildings. Illuminances are calculated from the irradiances using the luminous efficacy model from Olseth and Skartveit (1989). The luminous efficacy describes the conversion of irradiance to illuminance. The model is based on the CIE (International Commission on Illumination) curve for photopic vision and on spectral irradiances obtained by an interpolation between transmittance models for cloudless skies (Bird & Riordan, 1986) and unbroken cloud cover (Stephens, Ackerman, & Smith, 1985). The model has been parameterized and requires solar

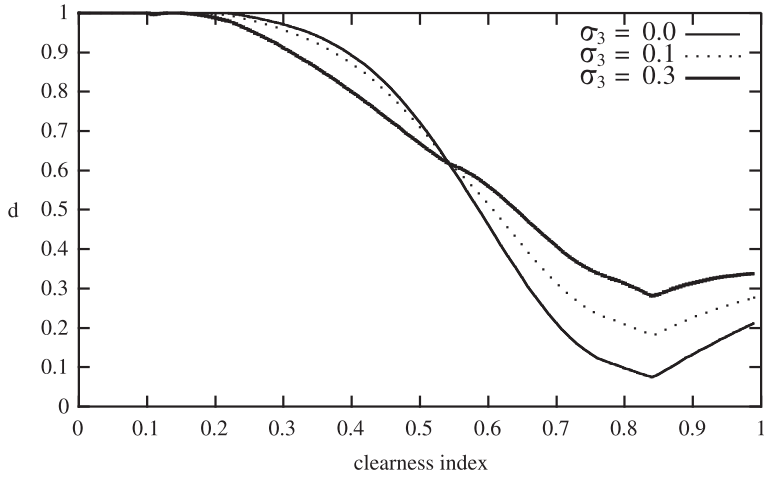

Fig. 4. Diffuse fraction d versus clearness index k_T, variability index $\sigma_3 = 0.0$, 0.1 and 0.3 for a solar zenith angle of 40° (Skartveit et al., 1998).

elevation, the day of year and diffuse and direct normal clearness indices as input.

3. Applications

In this section some example applications of satellite-derived irradiance are presented, which are convenient for urban planning. The examples result from recent European research projects (Sections 3.1 and 3.2) which aim at providing application-specific data mainly for the solar energy community and from current research of using satellite images for the production of additional information like forecasted irradiances.

3.1. Satel-Light—daylight usage in buildings

Within the framework of the *Satel-Light* project, a data base of solar radiation and daylight information for Western and Central Europe has been made available on the Internet. The data is completely derived from METEOSAT satellite imagery. Irradiances and illuminances covering a 2-year period (1996–1997) have been calculated on a half-hourly basis and a spatial grid of 10 km. For this purpose the HELIOSAT method has been largely modified and improved as described in Section 2.

The *Satel-Light* web server basically consists of pre-calculated cloud index values (Eq. (16)) and a set of numerical routines for the calculation of global and diffuse irradiance and illuminance values on horizontal and tilted surfaces frequencies for the occurrence of sky types and probabilities for exceeding given threshold values on different time scales. The data can be supplied by the server either as site-specific time series or statistics, or as graphical output in customized maps. For the latter purpose the server also features a basic set of GIS functionality.

A special motivation for the *Satel-Light* project was the scarcity of available daylight measurements. A good understanding of the site-specific daylight climate is essential for an optimal use of natural lighting in buildings for a reduction of overall energy consumption and a more comfortable indoor climate. The period covered by *Satel-Light* will be extended to 5 years (1996–2000) within the *SoDa* project (Section 3.2).

Fig. 5 shows maps representing the spatial information on the *Satel-Light* server. Here the annual global mean irradiance on a horizontal surface and the direct horizontal irradiance for the month of June are shown. In Fig. 6 another direct output of the server presents the frequencies of direct illuminance on a vertical plane oriented to the south (e.g. a window).

3.2. SoDa—integrated access to solar radiation and related data

The project *SoDa* (http://www.soda-is.com) aims at the integration of databases on solar radiation and other related information available on the Internet. Usually proprietary

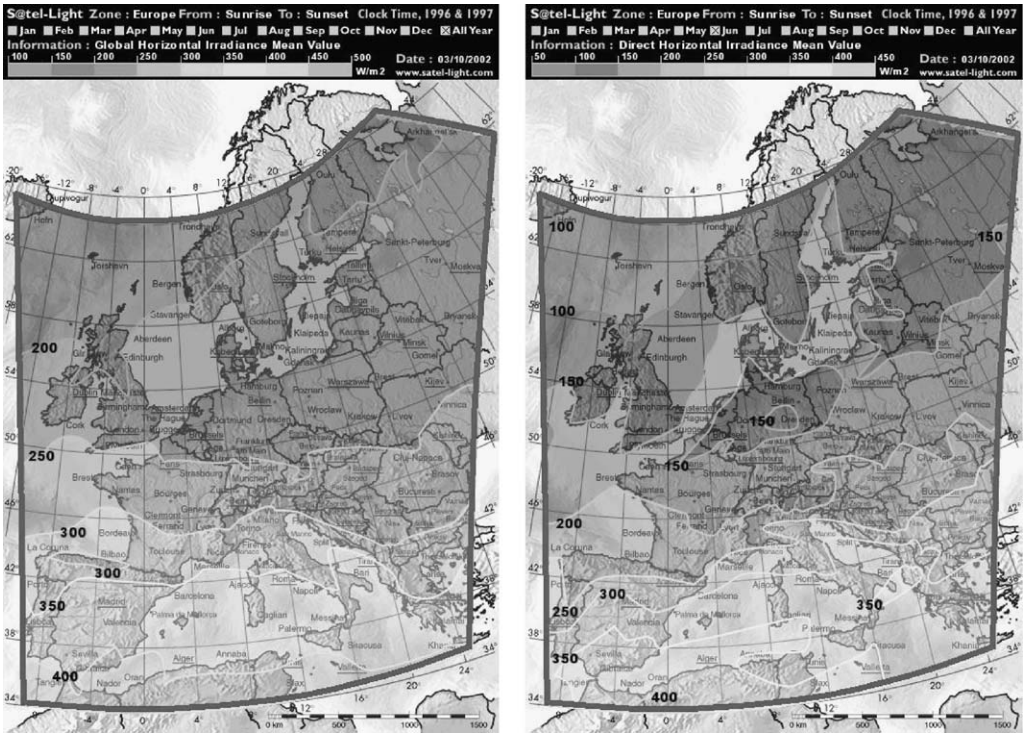

Fig. 5. Maps representing spatial information retrieved from the *Satel-Light* database. The annual mean of global irradiance on a horizontal surface (left) and the monthly (June) mean of direct horizontal irradiance (right) are shown. Both maps are based on 1996–1997 data averaged over the sunshine duration.

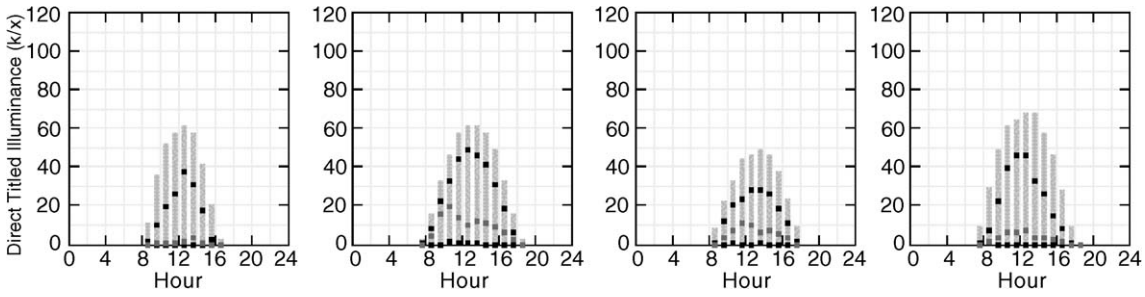

Fig. 6. Monthly frequencies of direct illuminance on a vertical, south-oriented surface for Berlin, Germany, retrieved from the *Satel-Light* data base. The months are January, April, July and October 1996–1997 (from left to right) showing hourly results (max (100%), 75%, 50% and 25%).

data formats and access procedures prevent potential users from an efficient use of these sources. The *SoDa* service will set up a unique portal for the end user and collect the data from existing data bases according to the needs of the user. Most of the data accessible through *SoDa* is derived from satellite-based services benefiting from the excellent spatial resolution of this source. This service is still under development and is supposed to be finished by the end of 2002. Until then prototype system can be accessed.

To demonstrate the usefulness of this new approach an example describing the application of *SoDa* is presented in the following. It focuses on the generation of an appropriate input data set for simulation purposes. Commonly used simulation tools often need hourly time series of solar irradiance and temperature as input as these variables determine energy production and performance of both solar thermal and electric systems.

In this case the *SoDa* system will combine radiation data derived from satellite imagery as described in Section 2 from the *Satel-Light* server, daily maximum and minimum temperatures from another internet database and a model developed by Dumortier (2002) to compute hourly temperature values which show a statistically correct correlation with the irradiance data. The combined time series then are ready for use in system simulation.

As a simple example of such an analysis a cost estimate of a solar thermal water heating system has been carried out. The costs of such a system are partly fixed, as the installation, the hot water storage, piping and regulators and partly variable due to the size of the collector field itself. In our analysis the field size is varied from 1 to 10 m^2. The analysis is done for Oldenburg in Germany (53.15°N, 8.17°E) with a system model which is also available on the *SoDa* webserver. The collector field is oriented to the south with a tilt angle of 45°. Further inputs are the hot water demand (200 l/day) and a temperature increment of (30 °C).

The results in Fig. 7 show decreasing relative costs with increasing system size for a small collector field, due to the dominating fixed costs. For large systems, however, the collector produces surplus heat and therefore reduces efficiency as is indicated by the decreasing slope of the solar fraction curve. The solar fraction is the share of energy supplied by the solar collector compared to the total energy demand. In our example the optimum is about 5 m^2 of collector area.

3.3. Solar irradiance forecasting

Forecasts of solar irradiance are an important input for intelligent operating strategies for any kind of solar energy

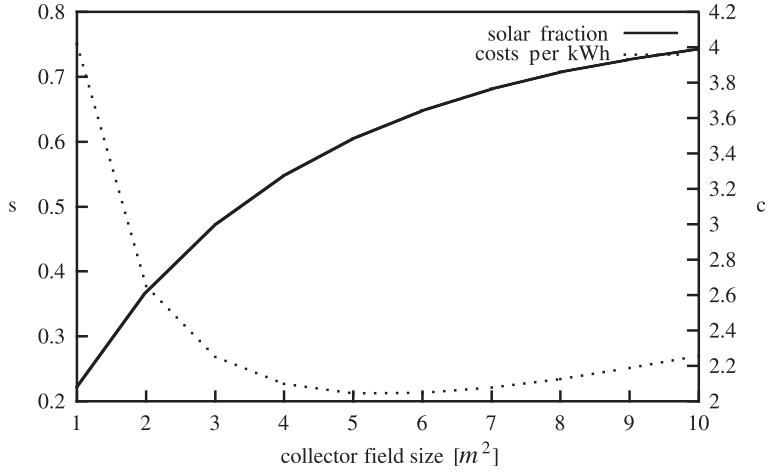

Fig. 7. Costs *c* per kWh of thermal energy (in arbitrary units) and solar fraction *s* for a solar hot water system versus collector field size. The web-based calculation has been done using satellite derived irradiance data.

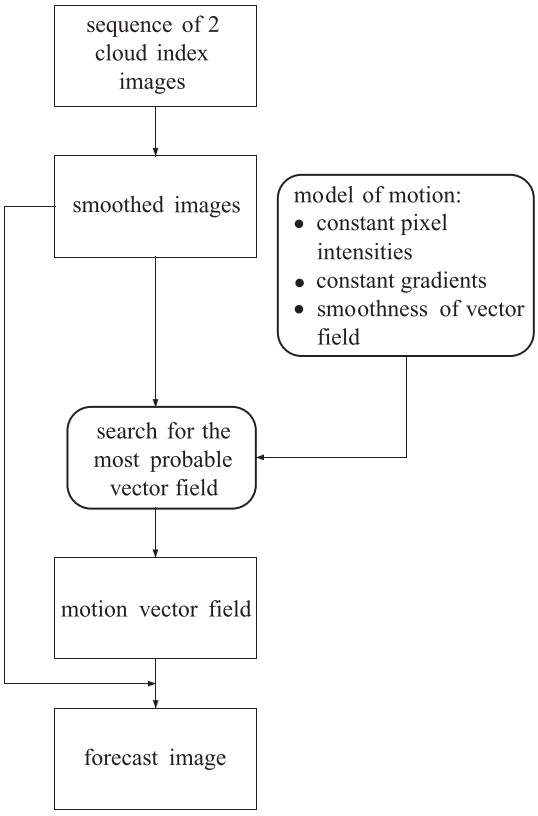

Fig. 8. Schematic diagram of the forecast method.

system. Depending on the application the information is required on different time scales. For very short forecast horizons of up to 2 h satellite images, providing information on radiation with high spatial and temporal resolution, are an appropriate source.

As cloudiness is the most important parameter influencing surface irradiance, the description of the temporal development of the cloud situation is the most essential part in irradiance forecasting. The forecasting routine presented here therefore focuses on the motion of clouds as the dominant phenomena with this respect. A more detailed description of this algorithm is given in Hammer, Heinemann, Lorenz, and Lückehe (1999).

A statistical method for the estimation of cloud motion is used to determine motion vector fields from two consecutive images, as shown in Fig. 8. In a first step the images are smoothed, because only large structures are preserved from one image to the next. To find a displacement field that describes best motion of the cloud structures, each displacement field is characterized by a probability function and the motion vector field with maximum probability is searched for. The probability for a given vector field is specified in a model of motion with the following assumptions, where the displacement field is denoted as d, the images as g_0 and g_1 and the position in the image as x_i:

- Pixel intensities are almost constant during motion,

$$U_1 = \sum_i [g_1(x_i + d(x_i)) - g_0(x_i)] \text{ is small.} \quad (22)$$

- Gradients of pixel intensities are almost constant,

$$U_2 = \sum_i [\nabla g_1(x_i + d(x_i)) - \nabla g_0(x_i)] \text{ is small.} \quad (23)$$

- The displacement field is smooth, neighboring vectors (i, $j \in \mathbb{N}$) do not differ much from each other,

$$U_3 = \sum_{i,j \in \mathrm{N}} |\mathrm{d}(x_i) - \mathrm{d}(x_j)|^2 \text{ is small.} \quad (24)$$

The probability $P(\mathrm{d} \mid g_0, g_1)$ of a vector field then can be described as:

$$P(\mathrm{d} \mid g_0, g_1) = \frac{1}{Z} \mathrm{e}^{-U} \quad (25)$$

with $U = U_1 + U_2 + U_3$ and Z a normalization constant. The most probable vector field is found by minimizing the energy function U. This is done with the statistical method of simulated annealing.

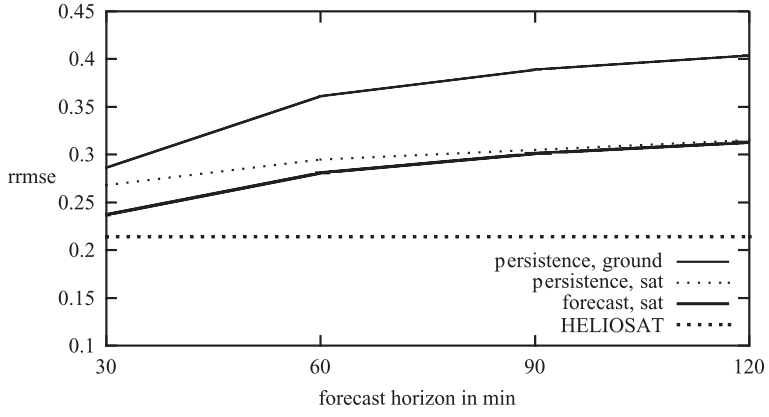

Fig. 9. Relative rmse (rrmse) of irradiance forecast as a function of the forecast horizon for a single station.

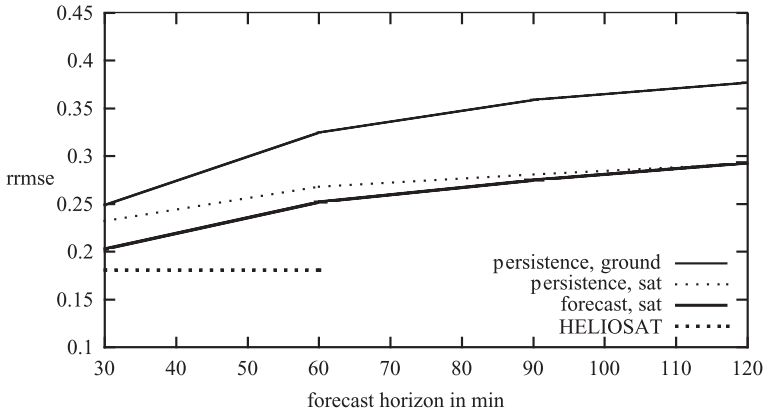

Fig. 10. Relative rmse (rrmse) of irradiance forecast as a function of the forecast horizon for an ensemble of eight stations distributed over an area of 5×7 km^2.

To forecast cloud index images the calculated motion vector field is applied to the current image, i.e., the motion is extrapolated into the future. The forecast quality is significantly improved by smoothing the images, the optimum size of the smoothing mask increases with the forecast horizon. The forecast of half-hourly mean values of the irradiance then is obtained by converting the predicted cloud index values to irradiance values using the HELIOSAT method.

The forecast quality was evaluated by comparisons with ground data for two different cases, single points and small regions (Figs. 9 and 10) (details see Hammer, Heinemann, Hoyer, & Lorenz, 2001). These cases correspond to different scales of applications: Local users, like management of a building, need point forecasts and large-scale applications, e.g. the grid integration of photovoltaics, benefit from area-averaged forecasts.

As a measure of forecast quality the rms-error was calculated for a time series of 50 days (14.5.97–2.7.97) and normalized with the mean irradiance during this period. Forecast errors were compared to ground persistence, where the current values of ground measurements are taken as forecast and to satellite persistence, where the ground radiation is derived from the smoothed current satellite image. As a lower limit the error of the HELIOSAT method itself (without forecast) is given. In both cases the global irradiance forecast shows smaller errors than persistence of satellite derived values. Due to the spatial information included in the satellite-derived values, they give significantly better results than ground persistence.

4. Perspectives opened by MSG

The current HELIOSAT method for calculating the solar irradiance from satellite imagery is well established and provides high-quality solar irradiance data. Nevertheless with the successful launch of the new European meteorological satellite MSG (Meteosat Second Generation) in August 2002 a significant increase in the accuracy of the calculated solar irradiance is expected.

The instrumental setup of MSG offers additional spectral channels and a higher spatial and temporal resolution. The HELIOSAT method will benefit in two areas by the enhanced capabilities of MSG. The larger number of channels will allow a more detailed remote sensing of the atmospheric state which will lead to a better description of the radiative transfer through the atmosphere. The higher spatial and temporal resolution will be helpful in a more accurate cloud detection. A new HELIOSAT method is currently developed in the EU-funded project *HELIOSAT-3* (http://www.heliosat3.de).

From the viewpoint of urban planning the benefits of a MSG-based calculation scheme will be the enhanced information about the spatial structure, the spectral distribution of solar irradiance as well as the angular distribution of diffuse light. The latter is of high importance for an optimal design of natural light systems, e.g., in large office buildings whereas knowledge of the spatial structure will be beneficial for the large-scale grid integration of photovoltaics.

To achieve these goals, the current semi-empirical HELIOSAT method will be improved by the introduction of a new type of calculation scheme based on radiative transfer modeling. This extension allows utilising the enhanced capabilities of MSG.

To model the radiative transfer within the atmosphere detailed knowledge of atmospheric parameters involved in scattering and absorption of the sunlight (e.g., aerosols and water vapor) is necessary for an accurate calculation of the solar irradiance. MSG will provide the potential for the retrieval of atmospheric parameters such as ozone, water vapor and—with restrictions—aerosols. Other platforms like GOME/ATSR-2 will be used in addition for the retrieval of aerosols. The explicit use of a radiative transfer model within the calculation scheme enables the direct calculation of user-specific irradiance information.

This calculation scheme will be used instead of the turbidity model in the current HELIOSAT method. As a

consequence an increase in the accuracy of the estimated relationship between diffuse and direct irradiance in clear sky situations is expected.

Moreover with the use of a radiative transfer model more precise information about the spectral and angular distribution of radiation will be achieved.

This is clearly related to the needs of urban planning, since accurate angular and spectral resolved solar irradiance data is a prerequisite for the optimum usage of sunlight and hence an energy-efficient planning of buildings.

Within the cloud transmission scheme MSG will make the estimation of cloud height and types possible, which enables the treatment of cloud shadow effects and increase the accuracy of the estimated cloud index. The higher spatial and temporal resolution will also allow a better detection of broken clouds, which will lead to a better estimation of diffuse and direct fractions.

Using the enhanced capabilities of MSG, solar irradiance data with higher accuracy, higher spatial and temporal resolution and a large geographical coverage will be provided in the near future.

5. Conclusion

The reduction of energy consumption especially in urban environments will constitute one of the major global challenges in the future. Planning of energy-efficient buildings and cities as well as an intelligent operation of their energy supply systems will become of primary importance. It is clear that both, planning and operation, strongly depends on the availability of accurate information on the governing boundary conditions. As a consequence, the introduction of solar energy technologies implies a detailed knowledge of the solar resource.

Depending on the application, the data have to be precise, on-time, with high spatial and temporal resolution, application-specific, and easily accessible. The attempts which have been made to introduce remote sensing data as a primary data source for solar energy applications are promising. Future satellite platforms combined with more advanced estimation methods give remote sensing data the potential of serving most of the above mentioned needs.

References

Beyer, H. G., Costanzo, C., & Heinemann, D. (1996). Modifications of the Heliosat procedure for irradiance estimates from satellite data. *Solar Energy*, *56*, 121–207.

Bird, R., & Riordan, C. (1986). Simple solar spectral model for direct and diffuse irradiance on horizontal and tilted planes at the earth's surface for cloudless atmospheres. *Journal of Climate and Applied Meteorology*, *25*, 87–97.

Bourges, B. (1992). Yearly variations of the Linke turbidity factor. *Climatic data handbook of Europe* (pp. 61–64). Dordrecht: Kluwer Academic Publishing.

Cano, D., Monget, J., Albuisson, M., Guillard, H., Regas, N., & Wald, L. (1986). A method for the determination of the global solar radiation from meteorological satellite data. *Solar Energy*, *37*, 31–39.

Commission of the European Communities, 2000. Green Paper: Towards a European strategy for the security of energy supply.

Dumortier, D., 1995. Modelling global and diffuse horizontal irradiances under cloudless skies with different turbidities. *Daylight II, jou2-ct92-0144, final report vol. 2*. Tech. rep., CNRS-ENTPE.

Dumortier, D., 2002. Prediction of air temperatures from solar radiation. Tech. rep., SoDa-5-2-4, CNRS-ENTPE.

Fontoynont, M., Dumortier, D., Heinemann, D., Hammer, A., Olseth, J., Skartveit, A., Ineichen, P., Reise, C., Page, J., Roche, L., Beyer, H. G., & Wald, L. (1997). *SATELLIGHT—processing of METEOSAT data for the production of high quality daylight and solar radiation available on a world wide web internet server, mid-term progress report, jor3-ct9-0041*. Tech. rep.

Fontoynont, M., Dumortier, D., Heinemann, D., Hammer, A., Olseth, J., Skartveit, A., Ineichen, P., Reise, C., Page, J., Roche, L., Beyer, H. G., & Wald, L. (1998). Satellite: A WWW server which provides high quality daylight and solar radiation data for Western and Central Europe. *9th conference on satellite meteorology and oceanography, Paris* (pp. 434–437).

Hammer, A., 2000. Anwendungspezifische Solarstrahlungsinformationen aus Meteosat-Daten. PhD Thesis, University of Oldenburg.

Hammer, A., Heinemann, D., & Hoyer, C. (2001). Effect of Meteosat VIS sensor properties on cloud reflectivity. *Third SoDa meeting, Berne (CH)*.

Hammer, A., Heinemann, D., Hoyer, C., & Lorenz, E. (2001). Satellite based short-term forecasting of solar irradiance—comparison of methods and error analysis. *The 2001 EUMETSAT meteorological satellite data user's conference* (pp. 677–684).

Hammer, A., Heinemann, D., Lorenz, E., & Lückehe, B. (1999). Short-term forecasting of solar radiation based on image analysis of meteosat data. *Proc. EUMETSAT meteorological satellite data users conference* (pp. 331–337).

Kasten, F. (1996). The Linke turbidity factor based on improved values of the integral Rayleigh optical thickness. *Solar Energy*, *56*, 239–244.

Kasten, F., & Young, A. (1989). Revised optical air mass tables and approximations formula. *Applied Optics*, *28*, 4735–4738.

Olseth, J., & Skartveit, A. (1989). Observed and modelled hourly luminous efficacies under arbitrary cloudiness. *Solar Energy*, *42*, 221–233.

Page, J., 1996. Algorithms for the Satellight programme. Tech. rep.

Renne, D. S., Perez, R., Zelenka, A., Whitlock, C., & DiPasquale, R. (1999). Use of weather and climate research satellites for estimating solar resources. *Advances in Solar Energy*, *13*.

Skartveit, A., Olseth, J., & Tuft, M. (1998). An hourly diffuse fraction model with correction for variability and surface albedo. *Solar Energy*, *63,* 173–183.

Stephens, G., Ackerman, S., & Smith, E. (1985). A short-wave parameterization revised to improve cloud absorption. *Journal of the Atmospheric Sciences*, *41*, 687–690.

Zelenka, A., Perez, R., Seals, R., & Renne, D. (1999). Effective accuracy of satellite-derived hourly irradiances. *Theoretical and Applied Climatology*, *62*, 199–207.